

# Observations Outside the Light-Cone: Algorithms for Non-Equilibrium and Thermal States

M. B. Hastings<sup>1,2</sup>

<sup>1</sup> *Center for Nonlinear Studies and Theoretical Division,  
Los Alamos National Laboratory, Los Alamos, NM, 87545*

<sup>2</sup> *Kavli Institute of Theoretical Physics, University of California, Santa Barbara, CA, 93106*

We apply algorithms based on Lieb-Robinson bounds to simulate time-dependent and thermal quantities in quantum systems. For time-dependent systems, we modify a previous mapping to quantum circuits to significantly reduce the computer resources required. This modification is based on a principle of “observing” the system outside the light-cone. We apply this method to study spin relaxation in systems started out of equilibrium with initial conditions that give rise to very rapid entanglement growth. We also show that it is possible to approximate time evolution under a local Hamiltonian by a quantum circuit whose light-cone naturally matches the Lieb-Robinson velocity. Asymptotically, these modified methods allow a doubling of the system size that one can obtain compared to direct simulation. We then consider a different problem of thermal properties of disordered spin chains and use quantum belief propagation to average over different configurations. We test this algorithm on one dimensional systems with mixed ferromagnetic and anti-ferromagnetic bonds, where we can compare to quantum Monte Carlo, and then we apply it to the study of disordered, frustrated spin systems.

## I. INTRODUCTION

Matrix product and density-matrix renormalization group methods provide one of the most powerful ways of simulating one-dimensional quantum systems. In addition to ground state properties[1], they have been extended to thermal and open systems[2] and dynamical problems[3]. The reason for the success of these algorithms is that in many cases the appropriate quantum state can be well-approximated by a matrix product state, giving a very compact representation of the state of the system.

In some cases, we even have theorems that quantify the accuracy of matrix product states. For ground states of local quantum systems with a gap, the ability to represent ground states as matrix product states follows from bounds on the entanglement entropies[4]. Related results are available for thermal systems[5, 6] and for non-equilibrium states obtained by starting with a factorized state and evolving under a local Hamiltonian for a time  $t$ ; in the first case the bond dimension needed to get a good matrix product approximation to the desired state scales exponentially in  $\beta$ , while in the second case it scales exponentially in  $t$ [7]. The two results [5, 7] are constructive proofs, which give an algorithm to find the matrix product state. All of these constructive proofs rely heavily on Lieb-Robinson bounds[8, 9, 10, 11].

In contrast to these constructive proofs, the matrix product algorithms used in practice are variational: they involve optimizing over different matrix product states to find the best one. This works well because in many practical cases the entanglement grows much more slowly than the upper bounds set by theory. For example, systems described by conformal field theory have an entanglement entropy growing only logarithmically with system size[12], while the area law bound[4] gives no useful result for these systems due to the absence of a gap. Similarly, for many initial conditions, evolution under a local Hamiltonian gives an entanglement entropy growing only logarithmically in time[13, 14, 15] while the theoretical upper bound gives an entanglement entropy growing linearly in time[16].

In this paper, we argue that there are many situations in which algorithms based on Lieb-Robinson bounds are the best technique. We first look at the case of time evolution in systems out of equilibrium. Here, there are initial conditions for which the entanglement entropy is known to grow linearly in time[17], in accordance with conformal field theory predictions[18]. Roughly speaking, logarithmic entropy growth tends to occur in cases where we can divide the chain into a small number of subchains such that the initial state is an eigenstate of the Hamiltonian on each subchain; for example, starting an XXZ spin chain in a state in which all the spins on the left half of the chain are up and all the spins on the right half of the chain are down leads to a logarithmic entropy growth[15]. On the other hand, the linear entropy growth tends to occur in cases where the initial state differs from an eigenstate of the Hamiltonian on every subsystem of the full spin chain. For example, starting an XXZ spin chain in an initial condition in which the spins alternate between up and down (a Neel state, the ground state when the Ising term is the only term in the Hamiltonian) leads to a linear entropy growth[17].

For system with linear entropy growth, matrix product methods will require a bond dimension growing exponentially in time to obtain accurate results. At this point, both variational matrix product and constructive, Lieb-Robinson-based methods require resources growing exponentially in time. The question, then, is how to obtain the smallest

exponential. To some extent, the Lieb-Robinson based methods (such as [7] and the methods below) are “worst-case”: the bond dimension depends on theoretical upper bounds for *arbitrary* local Hamiltonians, while the matrix product methods can adaptively find better representations. On the other hand, there are some disadvantages to matrix product methods. To get a rough idea of the resources required, let us consider a system of  $N$  spins, each of spin-1/2, with a local Hamiltonian. The simplest algorithm to simulate this system for a time  $t$  involves writing the initial condition down in some basis and then directly simulating it (we discuss below different methods for doing this), requiring resources scaling as  $2^N t$  using sparse matrix methods. A matrix product algorithm can avoid truncation error for this system by using matrices with bond dimension  $2^{N/2}$  [19, 20]. However, the algorithm must then perform singular value decompositions and eigenvalue calculations, taking a time which scales as the cube of these matrices, and hence of order  $2^{3N/2}$ , which is slower. Of course, the matrix product methods are really only useful if they are able to represent the system with a smaller bond dimension. In this case, though, even if such a representation exists, the algorithm must find it, and this can pose a problem. The algorithm for simulation of non-equilibrium systems depends on breaking the time evolution into a series of small Trotter steps; if the Trotter steps are too long this can lead to Trotter error, while if they are too short, the truncation error can grow rapidly: even if there is a good state the algorithm may not find it [15].

We can use this scaling of the difficulty with  $N$  to get an idea of the scaling of computation effort with time, using a Lieb-Robinson bound on the group velocity,  $v_{LR}$ . Suppose we wish to compute the expectation value of a local observable, such as a spin on a site, at a time  $t_f$ , starting from a factorized state at time  $t = 0$ . The number of spins in the past light-cone of this spin is  $2v_{LR}t$ , and the Lieb-Robinson bounds imply that the effect of spins outside the light-cone is exponentially small. Thus, it suffices to simulate only the dynamics of the  $N = 2v_{LR}t_f + O(\log(\epsilon))$  spins closest to the given spin in order to compute the expectation value to an accuracy  $\epsilon$ . This requires an effort scaling exponentially in time as  $t^2 2^{2v_{LR}t}$ . Similarly, if the entanglement entropy grows linearly in time, the matrix product methods also require an effort scaling exponentially in time.

Our main result in this paper is the light-cone quantum circuit algorithm, an application of the Lieb-Robinson bound that allows us to simulate the evolution of local observables with resources growing asymptotically as only  $Nt2^{v_{LR}}$ , by some statistical sampling. This allows twice as large systems as the direct method. We analyze the entropy growth in these systems and argue that matrix product methods are also less efficient for long time simulation. We apply the light-cone quantum circuit algorithm then to the problem of spin relaxation in spin chains started in the Neel state. The physical idea behind the light-cone quantum circuit algorithm is as follows: to find the state of a given spin at a time  $t_f$ , we only have to track the dynamics within the past light-cone of the spin. For times  $t$  close to zero, the past light-cone includes roughly  $2v_{LR}t_f$  spins, but at these early times the entanglement is small and hence the computational effort should be less. For times  $t$  close to  $t_f$ , the past light-cone includes few spins and hence should be easier to simulate.

The paper is organized as follows. We first derive the light-cone quantum circuit algorithm. We then apply it to spin relaxation, and study oscillations of the central spin, decay of the envelope of the oscillations, and also seemingly random oscillations of the central spin in chains where boundary effects become important. We then derive a related quantum circuit method, the corner transfer quantum circuit which may be useful for studying the evolution of global observables in highly entangled non-equilibrium states.

We then turn to a different problem, presenting one other application of Lieb-Robinson methods, using the quantum belief propagation algorithm [22] to study thermal states in disordered systems. The quantum belief propagation algorithm explicitly constructs a matrix product state for a thermal quantum system. While it manipulates operators, rather than states, and thus can be computationally expensive, it has other advantages. It has no Trotter error, making it fast and accurate at high temperatures: it can obtain quantities such as the susceptibility peak to higher accuracy using fewer resources than methods such as transfer matrix DMRG [23], although at low temperatures it breaks down, with the resources required scaling exponentially with the temperature. In this case, the exponential scaling with the temperature is again related to a linear relationship between a time scale, in this case  $\beta = 1/T$ , and a length scale. It can be applied to random systems, where transfer matrix DMRG cannot be used because of a lack of translation invariance. A good test of variational matrix product [2] methods on this kind of system is lacking, so we cannot compare here. We apply the quantum belief propagation algorithm to two random systems, one without frustration where we can compare to quantum Monte Carlo and one with frustration where Monte Carlo methods are not applicable.

## II. QUANTUM CIRCUIT METHODS

In this section we present the various quantum circuit methods. We begin by reviewing previous work, and then derive the light-cone quantum circuit algorithm, and apply it to a problem of spin relaxation. We then use previous results on the entanglement entropy growth to estimate the computational resources required for different approaches

to this problem, and finally we present the corner transfer quantum circuit method, an extension which allows access to global quantities.

### A. Background

To understand our algorithm, we first review the ideas in [7] which gives a construction of a matrix product operator approximation to the time evolution operator,  $\exp(-iHt)$ , using resources exponential in  $t$ . We consider a local Hamiltonian

$$H = \sum_i h_i, \quad (1)$$

where each  $i$  acts on sites  $i, i+1$ . This Hamiltonian obeys a Lieb-Robinson bound: given any operator  $O$  which has support on set of sites  $X$ , the operator  $\exp(iHt)O\exp(-iHt)$  can be written, with exponentially small error, as an operator acting on the set of sites  $i$  within distance  $v_{LR}t$  of  $X$ , where  $v_{LR}$  is the Lieb-Robinson group velocity.

To simulate the system for a time  $t$ , we divide the system into blocks of length  $l$ , where  $l$  is slightly larger than  $2v_{LR}t$  (the error in the approximation will be exponentially small in  $l - 2v_{LR}t$ ). We then let  $H = H_0 + H'$  where  $H_0$  is the sum of the Hamiltonians on each block and  $H'$  is the Hamiltonian connecting the blocks:

$$H_0 = \sum_k \sum_{i=kl+1}^{i \leq (k+1)l-1} h_i, \quad (2)$$

$$H' = \sum_k h_{kl}, \quad (3)$$

where the sum ranges over integers  $k$ .

We then write

$$\exp(-iHt) = \left( \mathcal{T} \exp[-i \int_0^t \exp(-iH_0t') H' \exp(iH_0t')] \right) \exp(-iH_0t), \quad (4)$$

where  $\mathcal{T}$  denotes that the exponential is time-ordered. The operator  $\exp(-iH_0t)$  is equal to the product  $\prod_k U_k$ , where  $U_k$  is a unitary operator acting on sites  $kl+1, kl+2, \dots, kl$ :

$$U_k = \exp(-i \sum_{i=kl+1}^{i \leq (k+1)l-1} h_i t). \quad (5)$$

Using the Lieb-Robinson bounds, we can approximate  $\exp(-iH_0t') h_{kl} \exp(iH_0t')$  by an operator  $h_{kl}(t')^{loc}$  which has support on sites  $kl - l/2 + 1, \dots, kl + l/2 - 1$  for  $|t'| \leq t$  and for  $l > v_{LR}t$ . Then the operator  $\mathcal{T} \exp[-i \int_0^t \exp(-iH_0t') H' \exp(iH_0t')] can then be approximated by a product  $\prod_k V_k$  where$

$$V_k = \mathcal{T} \exp[-i \int_0^t h_{kl}(t')^{loc}]. \quad (6)$$

The key in this construction is that the intervals  $kl - l/2 + 1, \dots, kl + l/2 - 1$  do not overlap for different  $k$ . This construction expresses the time evolution as a quantum circuit:

$$\exp(-iHt) \approx \prod_k V_k \prod_k U_k. \quad (7)$$

The support of the operators  $U_k, V_k$  and the circuit is shown in Fig. 1.

Precise error bounds can be given using Lieb-Robinson bounds for the error in Eq. (7). To get an error of order  $\epsilon$  in the propagator (7), we only need to take  $l = 2v_{LR}t + \mathcal{O}(\log(N/\epsilon))$ . In what follows, we will not make detailed error estimates, since Lieb-Robinson error estimates are fairly simple and are by now standard in the literature; when we say that it suffices to take a length scale “of order”  $v_{LR}t$  to obtain an approximation to a given local quantity, we mean that by taking the length scale  $v_{LR}t + \mathcal{O}(\log(N/\epsilon))$  we can obtain an error of order  $\epsilon$  in the state; when we are computing

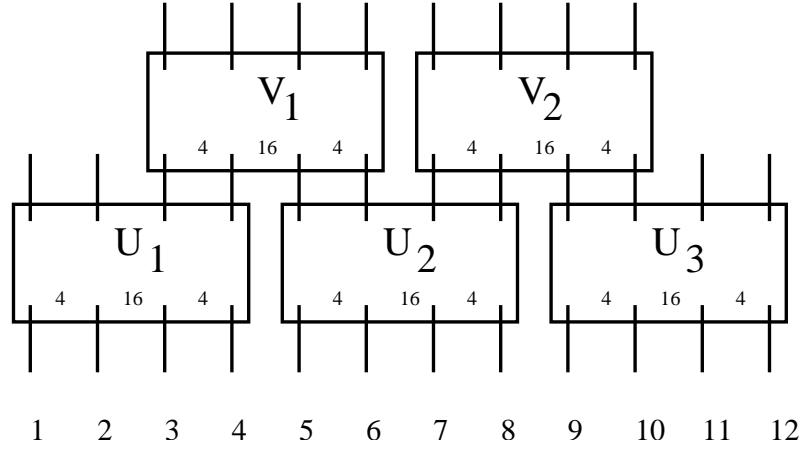


FIG. 1: Support of the operators  $U_k, V_k$  and the quantum circuit for  $N = 12$ ,  $l = 4$ . The small numbers at the bottom of operators  $U_k, V_k$  represent the bond dimensions required to represent these operators as matrix product operators; the maximum product of these across any bond is  $16 = 4^{l/2}$ .

expectation values of local quantities, to obtain an error of order  $\epsilon$  we need a length scale  $v_{LR}t + O(\log(v_{LR}t/\epsilon))$ , so that the error bound does not depend on  $N$  in this case.

Suppose we want to apply the quantum circuit procedure to compute the time evolution of some state  $\Psi_0$ . For simplicity, let  $\Psi_0$  be a factorized state (later we discuss the case where  $\Psi_0$  is a matrix product state both in this procedure and using our algorithm, and we find that using the idea of “observation” discussed below the case of matrix product state initial conditions presents no additional difficulty). The operator  $U_k$  is an operator acting on  $2l$  sites. Any such operator can be written as a matrix product operator with a bond dimension equal to  $4^{2l/2} = 2^{2l}$ [19]. This maximum bond dimension is achieved halfway across the interval of length  $2l$ , while at any point a distance  $d$  from one of the ends of the interval the bond dimension is only  $2^d$ , as shown in Fig. 1.

The same holds for  $V_k$ , and so the maximum product of bond dimensions across any bond is  $2^{2l}$  (a slightly worse estimate of  $2^{4l}$  was found for this construction in [7] since the fact that the bond dimension may vary with position was not taken into account).

There are several problems, however, with implementing the above method in practice, and it is these problems which we overcome with our methods, the light-cone quantum circuit method and the corner transfer quantum circuit method. The first method is most appropriate for computing local quantities (such as a spin or energy expectation value) while the second method is most appropriate for finding a good global approximation to the ground state.

The first problem is that operator equations of motion are computationally expensive in practice. To this end, we will modify the procedure to deal only with state vectors, rather than operators. The second problem is that the velocity of the quantum circuit does not obviously match the Lieb-Robinson velocity, in the following sense: given *arbitrary* operators  $U_k, V_k$ , supported as described above, the product  $\prod_k V_k \prod_k U_k$  can propagate information by a distance of  $2l$  in each time step. Since  $l$  is roughly  $v_{LR}t$ , this means that such a quantum circuit could have an effective velocity roughly  $2v_{LR}$ . Of course, the operators  $U_k, V_k$  are not arbitrary operators, but still we would like to fix this problem; we will show how to do this with the corner transfer quantum circuit method below which also leads to improved estimates on the maximum matrix product state dimension needed.

However, the real problem with this method is that it doesn’t lead to any improvement over naive simulation when it comes to computing local observables. The main problem we consider in this section is the following: we start a spin chain at time  $t = 0$  in a factorized state  $\Psi_0$ , and then evolve under a local Hamiltonian for to a final time  $t_f$ , at which point we wish to compute some local observable, such as  $S_i^z$ , the  $z$ -expectation value of spin  $i$ . By the Lieb-Robinson bounds, we can approximate  $S_i^z(t)$  by considering only a subchain of the full chain: we consider only sites  $i - l, \dots, i + l$ , where  $l$  is slightly larger than  $v_{LR}t_f$ . We then define  $\Psi'$  to be the appropriate factorized state on this subchain and evolve  $\Psi'$  for a time  $t_f$  using the Hamiltonian  $H'$  acting on the subchain. We then compute  $\langle \Psi' | \exp(iH't_f) S_i^z \exp(-iH't_f) | \Psi' \rangle$ . Using sparse matrix methods to compute the time evolution of  $\Psi'$ , this requires a computational effort of order  $l2^{2l}$ , which scales as  $2^{2v_{LR}t_f}$ . The quantum circuit method discussed above would also require simulations on intervals of length  $2l$ , and hence leads to no improvement when computing this local quantity.

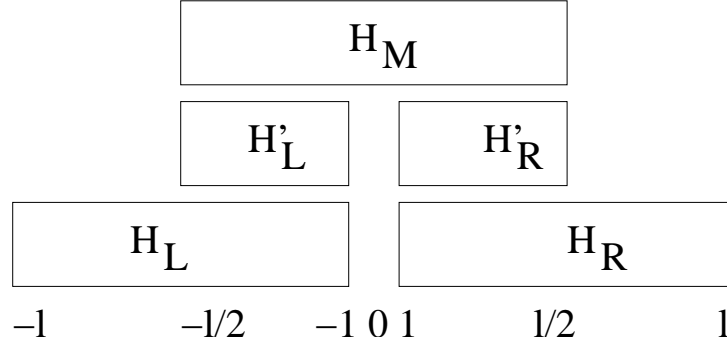


FIG. 2: Support of the operators  $H_L, H_R, H_M, H'_L, H'_R$ .

### B. Light-Cone Quantum Circuit Algorithm

We now show how to reduce the computational effort to an amount of order  $2^{v_{LR}t_f}$ , allowing the time scale to be twice as large, by combining Lieb-Robinson bounds with statistical sampling. While we focus on this section on starting in a factorized state, we later discuss the case of starting in a matrix product state.

We now derive our algorithm, which we call the light-cone quantum circuit method as it avoids keeping track of certain degrees of freedom outside the light-cone by making certain “observations” to reduce the computational effort. We first define a subchain of length  $2l + 1$  and an initial state  $\Psi'$  on that subchain as above. We label the sites in the subchain by  $-l, \dots, 0, \dots, +l$ . We let  $H'$  be the Hamiltonian on the subchain and we write

$$H' = H_L + H_R + H_B, \quad (8)$$

where  $H_L$  acts on the left half of the chain (sites  $-l, \dots, -1$ ),  $H_R$  acts on the right half of the chain, and the boundary Hamiltonian  $H_B$  acts on sites  $-1, 0, 1$ . Thus,  $[H_L, H_R] = 0$ . We define  $H_M$  to act on the *middle* half of the chain: it is supported on sites  $-l/2, \dots, +l/2$  (we pick  $l$  even for simplicity). See Fig. 2.

Using the Lieb-Robinson bounds in the same way as in the quantum circuit method above we can approximate the time evolution for a time  $t_i = t_f/2$  by:

$$\Psi'(t_f/2) = \exp(-iH't_f/2)\Psi' \approx \exp(-iH_M t_f/2) \exp[-i(H_M - H_B)t_f/2] \exp[iH_L t_f/2] \exp[iH_R t_f/2]\Psi'. \quad (9)$$

Note that the decomposition (9) is only good for times of order  $t_f/2$ . We wish to compute the expectation value of  $S_0^z$ , or any other observable on site 0, at time  $t_f$ . Again using the Lieb-Robinson bounds, the expectation value of this is approximately equal to

$$\langle \Psi'(t_f/2) | \exp(iH_M t_f/2) O \exp(-iH_M t_f/2) | \Psi'(t_f/2) \rangle. \quad (10)$$

Combining Eqs. (9,10) and our use of the Lieb-Robinson bounds to approximate the expectation value of  $O$  on the full chain by its expectation value on the subchain, we have

$$\langle \Psi_0 | O(t) | \Psi_0 \rangle \approx \langle \tilde{\Psi} | O | \tilde{\Psi} \rangle, \quad (11)$$

where

$$\tilde{\Psi} = \exp(-iH_M t_f/2)\Psi' \approx \exp(-iH_M t_f) \exp[-i(H_M - H_B)t_f/2] \exp[iH_L t_f/2] \exp[iH_R t_f/2]\Psi'. \quad (12)$$

The operator  $H_M - H_B$  is a sum of two operators,  $H'_L$  and  $H'_R$ , where  $H'_L$  acts on sites  $-l/2, \dots, -1$  and  $H'_R$  acts on sites  $+1, \dots, +l/2$ . Therefore,

$$\tilde{\Psi} = \exp(-iH_M t_f/2)\Psi' \approx \exp(-iH_M t_f) \left( \exp[iH'_L t_f/2] \exp[-iH_L t_f/2] \right) \left( \exp[iH'_R t_f/2] \exp[-iH_R t_f/2] \right) \Psi'. \quad (13)$$

Eq. (13) is not yet useful computationally, since it will require an effort of order  $lt_f 2^{2l}$  to compute the evolution of the state  $\Psi'$ . We now describe the light-cone quantum circuit method to compute the expectation value: first, write

$$\Psi' = \Psi_L \otimes \Psi_C \otimes \Psi_R, \quad (14)$$

where  $\Psi_L, \Psi_R$  are states on the left and right half of the chain, and  $\Psi_C$  is a state on the center site. We compute the states

$$\Psi'_L = (\exp[iH'_L t_f/2] \exp[-iH_L t_f/2]) \Psi_L, \quad (15)$$

and

$$\Psi'_R = (\exp[iH'_R t_f/2] \exp[-iH_R t_f/2]) \Psi_R, \quad (16)$$

which requires an effort of order  $lt_f 2^l$ . Next, we introduce a complete orthonormal basis of states on the sites  $-l, \dots, -l/2 - 1$ , which we label  $\phi_L(\alpha)$ , and another a complete basis of states on sites  $l/2 + 1, \dots, +l$  labelled  $\phi_R(\alpha)$ . Then we decompose  $\Psi'_L$  and  $\Psi'_R$  as:

$$\begin{aligned} \Psi'_L &= \sum_{\alpha} A(\alpha) \phi_L(\alpha) \otimes \xi_L(\alpha), \\ \Psi'_R &= \sum_{\alpha} A(\alpha) \phi_R(\alpha) \otimes \xi_R(\alpha), \end{aligned} \quad (17)$$

where  $\xi_L(\alpha)$  is some normalized state on sites  $-l/2, \dots, -1$  and  $\xi_R(\alpha)$  is some normalized state on sites  $+1, \dots, +l/2$ . The states  $\phi_L(\alpha)$  need not be eigenvectors of any reduced density matrix and the states  $\xi_L(\alpha)$  need not be orthogonal to each other, as Eq. (17) is *not* a Schmidt decomposition. Thus, from Eqs. (13,15,16,17),

$$\langle \tilde{\Psi} | O | \tilde{\Psi} \rangle = \sum_{\alpha_L} \sum_{\alpha_R} |A(\alpha_L)|^2 |A(\alpha_R)|^2 E(O, \alpha_L, \alpha_R), \quad (18)$$

where

$$E(O, \alpha_L, \alpha_R) = \langle \xi_L(\alpha_L) \otimes \Psi_C \otimes \xi_R(\alpha_R) | \exp(iH_M t_f) O \exp(-iH_M t_f) | \xi_L(\alpha_L) \otimes \Psi_C \otimes \xi_R(\alpha_R) \rangle. \quad (19)$$

Eq. (18) is at the heart of the light-cone quantum circuit approach. Numerically we proceed as follows: first, we compute  $|A(\alpha_L)|^2$  and  $|A(\alpha_R)|^2$  for all  $\alpha_L, \alpha_R$ . This requires an effort of order  $2^l$ . We then do a statistical sampling: we randomly pick an  $\alpha_L$  and an  $\alpha_R$  according to the probability distributions  $|A(\alpha_L)|^2$  and  $|A(\alpha_R)|^2$ , and compute the average  $E(O, \alpha_L, \alpha_R)$ . We repeat this procedure many times, to average over different choices of  $\alpha_L, \alpha_R$ .

The computational effort required then scales as only  $l2^l$ , or roughly  $t2^{v_L R t}$  as claimed. Asymptotically this allows double the time. The time scales linearly in the number of iterations of statistical sampling, which we denote  $N_{it}$ . However, if  $O$  has bounded operator norm, then  $E(O, \alpha_L, \alpha_R)$  has bounded moments, and so by the central limit theorem, the number of iterations required still scales only polynomially in the error.

### C. Results on Non-Equilibrium Dynamics

We now discuss results from this method, as well as some implementation details. We consider evolution under the XXZ Hamiltonian

$$H = \sum_i (S_i^x S_{i+1}^x + S_i^y S_{i+1}^y + \Delta S_i^z S_{i+1}^z). \quad (20)$$

For  $\Delta = 0$ , this problem can be mapped to free fermions by a Jordan-Wigner transformation and solved exactly. We use this as a check on our results later.

We used as a starting point the Neel state, with spins alternating up and down, and we computed the time dependence of  $S^z(t)$  for the central spin. The main numerical effort is to compute the evolution of a state under a Hamiltonian, which we did using a combination of short steps with a series method. For example, to compute  $\exp(-iH_L t) \Psi_L$  we divide the time  $t$  into shorter intervals of time  $t_0$ , and compute  $\exp(-iH_L t_0) \Psi_L = \Psi_L - it_0 H_L \Psi_L - (t_0^2 H_L^2 / 2!) \Psi_L + \dots$ , keeping a fixed number of terms in this series. We then repeat this procedure  $(t/t_0)$  times. To obtain negligible error for a chain of 20 sites with  $t_0 = 1$  required going to roughly 40-th order for  $|\Delta| \leq 1$ , while for  $\Delta = 2$  slightly longer series were required. A more sophisticated way of doing the time evolution would be to build a tridiagonal Hamiltonian in the Krylov space spanned by  $\Psi_L, H_L \Psi_L, \dots, H_L^k \Psi_L$  for some  $k$ , and then evolve exactly with this Hamiltonian[25].

Another important point of numerical simulation is the use of symmetries. We can choose the states  $\phi_L(\alpha)$  and  $\phi_R(\alpha)$  to be eigenstates of total  $S^z$ . Then, since the state  $\Psi'$  is an eigenstate of total  $S^z$ , the state  $\xi_L(\alpha_L) \otimes \Psi_C \otimes \xi_R(\alpha_R)$

is also an eigenstate of total  $S^z$ , which allows us to use symmetries when computing the evolution of the state. Since most of the numerical time is consumed statistically sampling  $E(O, \alpha_L, \alpha_R)$ , we build the sparse matrix for the Hamiltonian  $H_M$  in each spin sector once, before doing the sampling, and then run the sampling.

It is also possible, although we did not implement it, to take into account reflection symmetry. Since  $\alpha_L$  and  $\alpha_R$  are chosen independently, the state  $\xi_L(\alpha_L) \otimes \Psi_C \otimes \xi_R(\alpha_R)$  does not have reflection symmetry. However, if both the Hamiltonian  $H_M$  and the operator  $O = S_i^z$  have reflection symmetry, then it is useful to write

$$\xi_L(\alpha_L) \otimes \Psi_C \otimes \xi_R(\alpha_R) = \Psi_S(\alpha_L, \alpha_R) + \Psi_A(\alpha_L, \alpha_R), \quad (21)$$

where  $\Psi_S, \Psi_A$  are symmetric and anti-symmetric states. Then,

$$\begin{aligned} E(O, \alpha_L, \alpha_R) = & \langle \Psi_S(\alpha_L, \alpha_R) | \exp(iH_M t) O \exp(-iH_M t) | \Psi_S(\alpha_L, \alpha_R) \rangle \\ & + \langle \Psi_A(\alpha_L, \alpha_R) | \exp(iH_M t) O \exp(-iH_M t) | \Psi_A(\alpha_L, \alpha_R) \rangle, \end{aligned} \quad (22)$$

and so we can statistically sample one of the two terms on the right-hand side of Eq. (22). Note that on each iteration we randomly choose an  $\alpha_L$  and an  $\alpha_R$  and then randomly choose a term in Eq. (22), rather than repeatedly sampling Eq. (22).

As the algorithm is described above, the initial computation of the states  $\Psi_L(\alpha)$  and  $\Psi_R(\alpha)$  depends on the final time. For each final time  $t$ , we have to compute a new set of states  $\Psi_L(\alpha)$  and  $\Psi_R(\alpha)$  and then do the statistical sampling. However, in fact, we can speed the algorithm up at a slight cost in accuracy: we fix a given  $t_f$  and on each statistical sample we compute the state

$$\exp(-iH_M t_f) | \xi_L(\alpha_L) \otimes \Psi_C \otimes \xi_R(\alpha_R) \rangle, \quad (23)$$

to evaluate the expectation value in Eq. (19). We then act on this state with the operator  $\exp(iH_M \delta t)$  for some small  $\delta t$ . We then use this new state to compute an approximation to the expectation value at time  $t_f - \delta t$ . We then act on that state with  $\exp(-iH_M \delta t)$  to compute an approximation to the expectation value at time  $t_f - 2\delta t$ , and so on. Since the computational cost of performing the time evolution of a state under a Hamiltonian is proportional to the time evolved, these additional steps are relatively cheap, for  $\delta t \ll t_f$ . There is a small cost in accuracy: in general, to compute expectation values at a time  $t$ , we can do the initial evolution for a time  $t_i$ , and then evolve further for time  $t - t_i$ . To make the effect of boundary conditions as small as possible, we would like to have both  $t_i$  and  $t - t_i$  as small as possible, which is why above we chose to evolve for a time  $t_i = t_f/2$ . However, if  $\delta t \ll t_f$ , then we are not far away from the ideal choice of  $t_i$  by initially evolving for time  $t_f/2$  and then evolving for time  $t_f/2 - \delta t$ . We followed this procedure in the numerical work below, with  $\delta t = 0.25$  and taking  $t_f$  to be spaced with integer steps using  $t_0 = 1$ . This accounts for some of the slight kinks in the curves after every integer value of  $t$ .

The spin-wave velocity of Hamiltonian (20) for  $\Delta \leq 1$  is given by

$$v_{sw} = (\pi/2) \sin(\theta)/\theta, \quad (24)$$

where  $\cos(\theta) = \Delta[24]$ . On the other hand, in the development above, we used a Lieb-Robinson velocity  $v_{LR}$ , where

$$v_{LR} \geq v_{sw}. \quad (25)$$

Using the Lieb-Robinson bounds, we showed that we could accurately simulate for a time  $t$  using length scales  $l = v_{LR} t$ . As mentioned above, we do not give precise error estimates, but it is not hard to give rigorous estimates of the error. However, the Lieb-Robinson bound is actually fairly conservative because of Eq. (25), and thus in practice length scales  $v_{sw} t$  suffice to get good results.

We begin by illustrating results for the XY chain, with  $\Delta = 0$ . In Fig. 3, we illustrate results from exact simulations of the XY chain for various sizes. We consider chains with open boundary conditions with  $N = 35, 51, 101$  and a chain with periodic boundary conditions with  $N = 36$ . For the chains with open boundary conditions, we plot the average of the central spin as a function of time, while for the periodic boundary conditions we plot the average of an arbitrarily chosen spin as a function of time. The large exact simulations are possible because this chain can be mapped to free fermions by a Jordan-Wigner transformation. Later we will present comparison of these results to light-cone quantum circuit results. For now, we discuss aspects of Fig. 3 which show the influence of boundary effects. In the range of times, the chain with  $N = 101$  shows no effect of the boundary. There are oscillations of the spin with frequency  $\omega$  roughly 2, with an envelope decaying as  $1/\sqrt{t}$  so as

$$\langle S_i^z \rangle \sim \frac{1}{\sqrt{t}} \cos(\omega t + \theta_0), \quad (26)$$

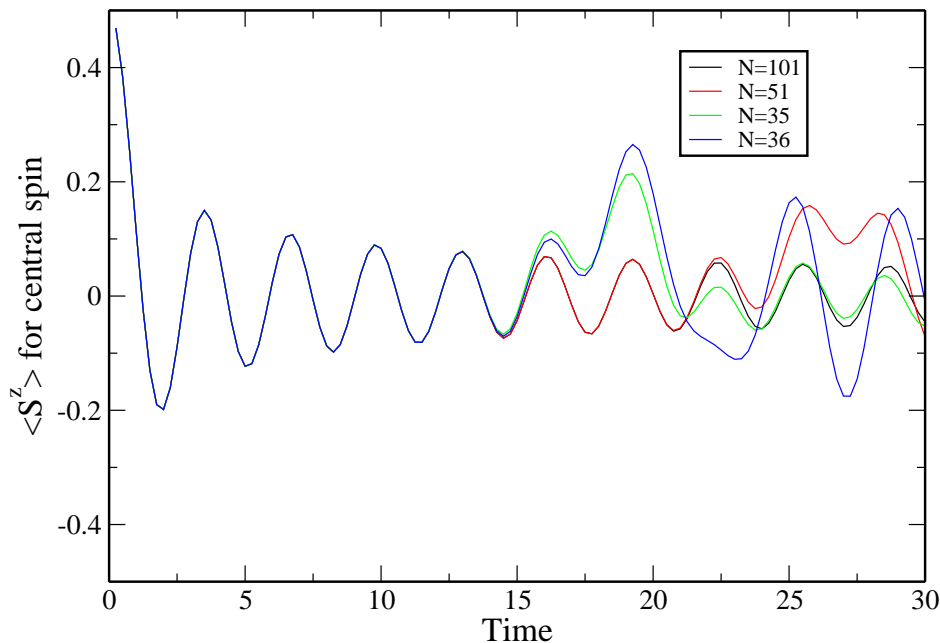


FIG. 3: Time dependence of  $\langle S^z \rangle$  for the central spin as a function of time. Curves are  $N = 101$  (black),  $N = 51$  (red),  $N = 35$  (green), and  $N = 36$  (blue).

for  $\theta_0 \approx (3/4)\pi$ . Simulations on longer chains show that as long as  $N$  is less than  $t/2$ , the decaying oscillations of Eq. (26) continue to hold. In regard to the  $1/t^{1/2}$  decay of oscillations found here numerically, it is interesting to note a similar power-law decay found for a different system of free bosons, where fluctuations about a maximal entropy state were proven to decay at least as fast as  $1/t^{1/3}$ [21].

For  $N$  larger than  $t/2$ , the boundary conditions become important, as one can see in the curves for  $N = 35$  and  $N = 51$ , which start to show deviations from the  $N = 101$  curve for times roughly 16 and 22 respectively. This is no surprise, since the distance between the central spin and the boundary is  $N/2$ , and  $v_{sw} = 1$  for  $\Delta = 0$ . We will see later for  $\Delta \neq 0$  that in general boundary effects become important for  $N/2 = tv_{sw}$ . Interestingly, periodic boundary conditions offer no improvement, since the  $N = 36$  periodic curve deviates at the same time as the  $N = 35$  open curve.

Another interesting effect is that once the boundary conditions become important, the expectation value shows wild oscillations, which no longer decrease in magnitude. This may be a consequence of the fact that the chain is integrable. It would be interesting to see for a non-integrable system whether such oscillations occur or not; the simplest statistical assumption for a non-integrable system is that the state at long times would be a random pure state satisfying the conservation laws of total  $S^z$  and total energy, and thus the expectation value of  $\langle S_i^z \rangle$  for any  $i$  would show only exponentially small fluctuations about the average spin.

We now consider the application of the light-cone quantum circuit method to this chain. We considered  $l = 18$  and 20, and did  $N_{it} = 1000$  iterations of statistical sampling, as shown in Fig. 4. The results for exact simulations with  $N = 35$  and  $N = 101$  are also shown for comparison. We see that the light-cone quantum circuit method with  $l = 18$  is accurate over the same range of times as the exact simulation with  $N = 35$ , while the light-cone quantum circuit method with  $l = 20$  improves on this result. By increasing  $l$  from 18 to 20, we increase the range of times by roughly 2, while increasing  $N$  by 2 would increase the range of times by only 1.

There are statistical fluctuations in the light-cone quantum circuit results in Fig. 4, due to random fluctuations in  $E(O, \alpha_L, \alpha_R)$  for different choices of  $\alpha_L, \alpha_R$ . In Fig. 5 we plot the rms fluctuation in  $E(O, \alpha_L, \alpha_R)$  as a function of time, sampling this expectation value with the probability distribution  $|A(\alpha_L)|^2 |A(\alpha_R)|^2$ . The results in Fig. 4 are an average over  $N_{it} = 1000$  samples, so the spread on each data point in Fig. 4 is equal to  $1/\sqrt{1000}$  times the fluctuation shown in Fig. 5, or roughly 0.005 in the worst case. A very interesting point is that for  $t \leq 5$ , the rms fluctuation is negligible, while for times  $t \geq 9$ , the rms fluctuations are up to their full value, with a sharp bend in the curve (plotted on a log scale) around  $t = 8$  or  $t = 9$ . This is a consequence of the maximum spin-wave velocity: the influence of the regions on sites  $-l, \dots, -l/2$  and  $+l/2, \dots, +l$  takes a time of order  $l/2v_{sw}$  to reach the central region. There are still some fluctuations for  $t \leq l/2v_{sw} = 9$ , but they decay rapidly until they are negligible at very short time.

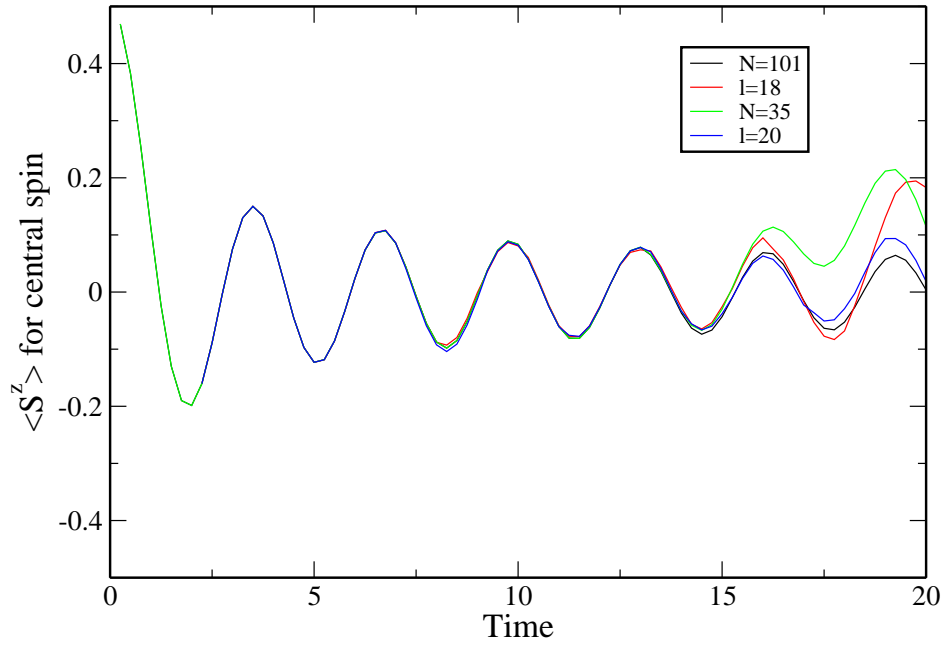


FIG. 4: Time dependence of  $\langle S^z \rangle$  for the central spin as a function of time for  $\Delta = 0$ . Exact curves are  $N = 101$  (black) and  $N = 35$  (green). Light-cone quantum circuit curves are  $l = 18$  (red) and  $l = 20$  (blue).

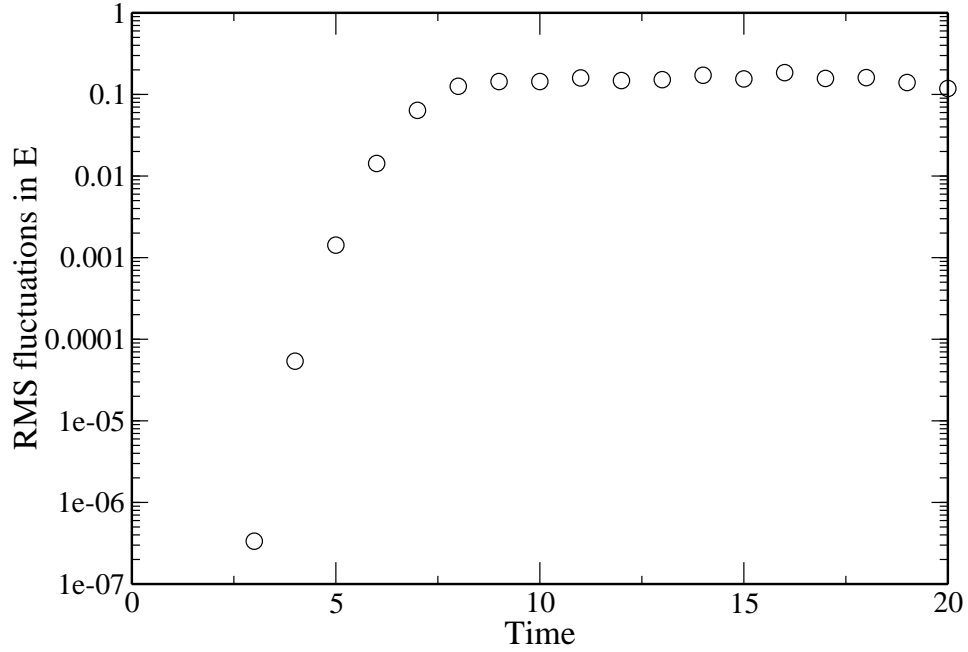


FIG. 5: RMS fluctuations in  $E(O, \alpha_L, \alpha_R)$  as described in text as a function of time for  $l = 18$ .

We then applied the light-cone quantum circuit method to chains with  $\Delta = 0.5, 1, 2$  as shown in Figs. 6,7,8. For comparison, we show an exact simulation of a chain with  $N = 20$ . For larger  $\Delta = 0.5, 1$  we still see decaying oscillations, but the decay is much more rapid than for  $\Delta = 0$ . The decay of the envelope is, very roughly,  $t^{-1.25}$  for  $\Delta = 0.5$ . For  $\Delta = 2$ , no oscillations are seen. The effects of statistical noise are much more noticeable, since the magnitude of the spin is much less. All simulations were done with  $N_{it} = 1000$  statistical samples, except the simulation with  $\Delta = 0.5, l = 22$  has only  $N_{it} = 250$  samples, and the simulations with  $\Delta = 1, l = 16$  and  $\Delta = 1, l = 18$

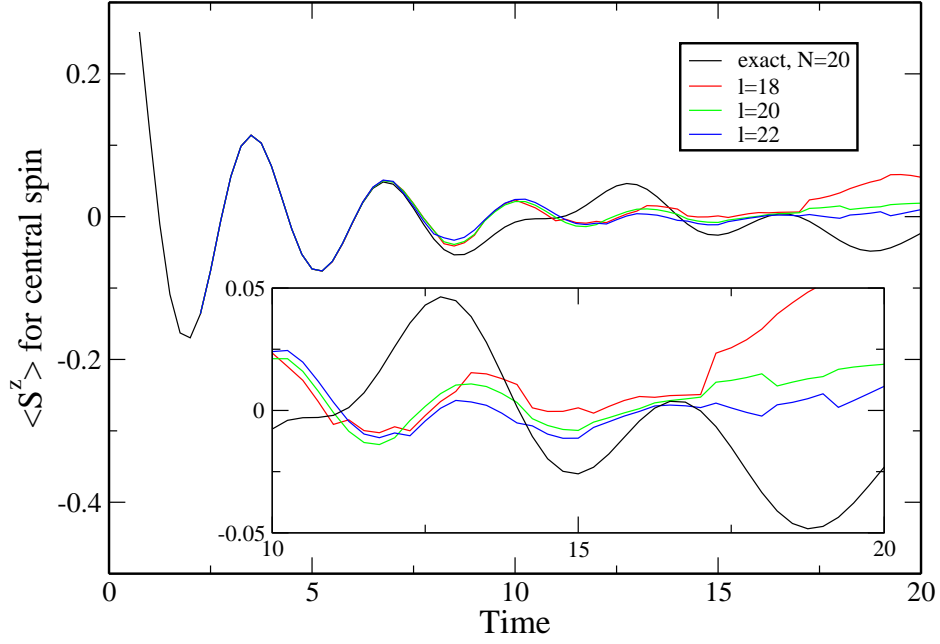


FIG. 6: Time dependence of  $\langle S^z \rangle$  for the central spin as a function of time for  $\Delta = 0.5$ . Exact curve is  $N = 20$  (black). Light-cone quantum circuit curves are  $l = 18$  (red),  $l = 20$  (blue), and  $l = 22$  (green).

had  $N_{it} = 10000$  and  $N_{it} = 3000$  samples respectively. The spin-wave velocity is larger for these chains, so the simulation breaks down at an earlier time than for  $\Delta = 0$ ; we again see that the simulations work for

$$t \lesssim N/(2v_{sw}), \quad (27)$$

or

$$t \lesssim l/v_{sw}, \quad (28)$$

in the exact and light-cone methods respectively.

#### D. Entanglement Entropy

From the predictions in [18] and the numerical work in [17], we can compare the difficulty of doing a similar calculation doing time-dependent DMRG or time evolving bond decimation. The entanglement entropy is predicted to grow linearly in time. In [17], the prefactor of the numerical growth was determined in a quench of an XXZ chain from an Ising coupling with  $\Delta = \Delta_0$  to an Ising coupling with strength  $\Delta_1$ . The prefactor depended on  $\Delta_0$  and was largest in the case of  $\Delta_0 = \infty$ , the case we have considered here where the initial condition is a Neel state. There, in a quench to  $\Delta_0 = 0$ , the entanglement entropy (with logs taken to base 2) was observed to grow a little faster than  $0.6v_{sw}t$ . This implies that the minimum size of the bond dimension needed in a matrix product state is at least  $2^{0.6v_{sw}t}$ , which requires an effort going as  $2^{1.8v_{sw}t}$ . In contrast, the numerical effort required to directly simulate a chain of length  $N$  scales as  $2^N$ . To get accurate results for a time of order  $t$ , requires  $N = 2v_{sw}t$ , or an effort  $2^{2v_{sw}t}$ . Using the techniques in the present paper, the effort can be reduced to of order  $2^{v_{sw}t}$ .

When comparing to [17], note that there is a difference in normalization of the Hamiltonian by a factor of 4, but since the results in [17] are expressed in terms of the spin-wave velocity multiplied by time, the time axis is the same for  $\Delta = 0$ . For  $\Delta > 0$ , the time axis in [17] differs from the time axis here, since [17] multiplies the time by the relevant spin-wave velocity which is greater than unity. For  $\Delta = 1$ , the spin-wave velocity using our normalization is equal to  $\pi/2 > 1$ , and for  $\Delta = 0.5$  the spin-wave velocity is equal to  $3\sqrt{3}/4$ , so the times in the present paper should be multiplied by such a factor greater than unity when comparing to [17].

In [17], other initial conditions were considered, other than just the Neel state. These initial conditions were chosen to be the ground state of various other XXZ Hamiltonians. As the initial  $\Delta$  was reduced, the entropy growth was

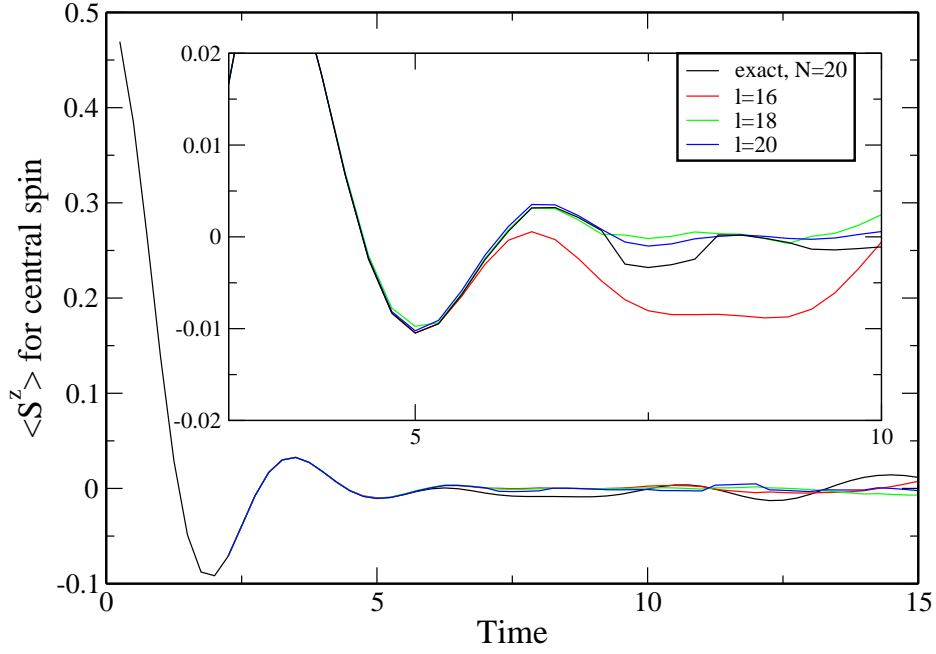


FIG. 7: Time dependence of  $\langle S^z \rangle$  for the central spin as a function of time for  $\Delta = 1$ . Exact curve is  $N = 20$  (black). Light-cone quantum circuit curves are  $l = 16$  (red),  $l = 18$  (green), and  $l = 20$  (blue).

found to still be linear in time, but with a smaller prefactor. Such simulations could still be carried out with our method as follows: first, use DMRG as done in [17] to find the ground state on a long chain. Then, suppose we are interested in local observable on a region of length  $l_0$ . To find how these evolve a time  $t$  after a quench, locate some region of length  $l_0 + 2vt$  in the chain.

We then “observe” the state of the system outside this region to statistically sample different pure states within the region, and then evolve the pure states within the region. This is done as follows. The DMRG ground state can be written in the form

$$\Psi_0 = \sum_{\alpha\beta} A_{\alpha\beta} |\Psi_L^\alpha\rangle \otimes |\Psi_M^{\alpha\beta}\rangle \otimes |\Psi_R^\beta\rangle, \quad (29)$$

where  $|\Psi_L^\alpha\rangle$  are a set of orthonormal states on the chain to the left of the region,  $|\Psi_R^\beta\rangle$  are a set of orthonormal states to the right of the region,  $|\Psi_M^{\alpha\beta}\rangle$  are a set of states (normalized to unity but not necessarily orthogonal) on the given region of length  $l_0 + 2vt$ , and  $A^{\alpha\beta}$  are a set of amplitudes. We choose an  $\alpha$  and a  $\beta$  according to the probability

$$P = |A^{\alpha\beta}|^2, \quad (30)$$

and then evolve the state  $|\Psi_M^{\alpha\beta}\rangle$  using our present algorithm. This corresponds to observing the matrix product state in the basis  $|\Psi_L^\alpha\rangle \otimes |\Psi_R^\beta\rangle$ . Repeating this statistical sampling many times we obtain the desired quantities on the local region. Note that on each iteration we statistically sample  $\alpha, \beta$  as well as doing the sampling above. The statistical sampling of the state outside the region may be justified using Lieb-Robinson bounds as before. Further, when a matrix product state is written in the canonical form, the bond variables naturally have the orthonormality property used above to do the statistical sampling, giving a state in the form (29).

In some cases, if the entanglement entropy grows linearly in time but with a sufficiently small prefactor, it may be worth using the light-cone ideas above, but doing the initial evolution for a time  $t_i$  using matrix product methods instead of quantum circuit methods, as follows. Suppose the matrix product methods require an effort  $t^2 2^{ft}$ , for some number  $f$ , to simulate for a time  $t$ . Then, to compute an observable at time  $t_f$ , we simulate a subchain of length  $2v_{sw}t_f$  for a time  $t_i$  using matrix product methods. We then statistically sample states on a smaller subchain of length  $2v_{sw}(t_f - t_i)$  and perform the simulation of that subchain for time  $t_f - t_i$  exactly. The total effort is then

$$t^2 O(2^{ft_i} + 2^{2v_{sw}(t_f - t_i)}). \quad (31)$$

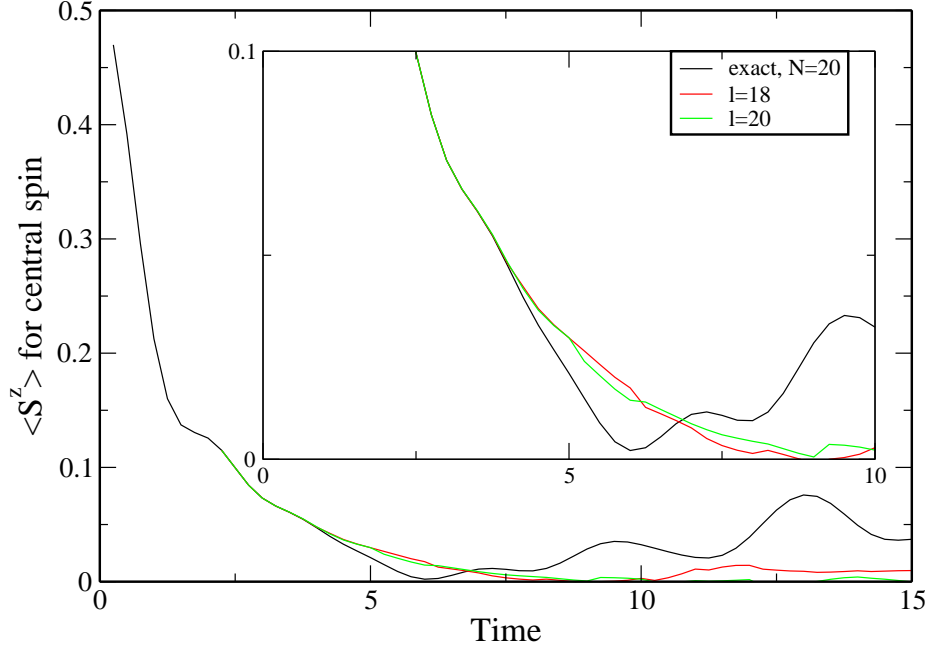


FIG. 8: Time dependence of  $\langle S^z \rangle$  for the central spin as a function of time for  $\Delta = 2$ . Exact curve is  $N = 20$  (black). Light-cone quantum circuit curves are  $l = 18$  (red) and  $l = 20$  (green).

Choosing  $t_i = t_f/(1 + f)$  to minimize the computational cost, we find that the cost scales as

$$t^2 O(2^{f' t_f}), \quad (32)$$

with

$$f' = \frac{1}{f^{-1} + (2v_{sw})^{-1}}. \quad (33)$$

### E. The Corner Transfer Quantum Circuit Method

In this subsection we introduce the corner transfer quantum circuit method. It is primarily of theoretical, rather than practical interest. For calculation of local quantities (such as the expectation value of the spin on a single site) the light-cone method above is less work. However, the corner transfer method does give an approximation to the full wavefunction, and may be less work than variational matrix product methods in cases where the entanglement entropy grows rapidly.

We now define the quantum circuit that approximates  $\exp(-iHt)$ . We define a length scale  $l' \ll v_{LR}t$ : the error in our quantum circuit approximation to  $\exp(-iHt/2)$  will be exponentially small in  $l'$ , while the maximal velocity of information propagation for our quantum circuit will be

$$v_{max} = v_{LR} + \mathcal{O}(l'/v_{LR}t). \quad (34)$$

We construct the quantum circuit in two steps, first presenting a quantum circuit that approximates  $\exp(-iHt/2)$ . We introduce operators  $U_k$  that describe the time evolution under a time dependent Hamiltonian: each  $U_k$  contains at a time  $t$  only the interaction terms which are contained within one of the triangles with a flattened top and jagged sides surrounded by a dashed line shown in in Fig. 9(a). That is, we break the time  $t/2$  into  $n_0 = \lceil v_{LR}(t/2) \rceil$  subintervals of time at most  $1/v_{LR}$ . We place the center of the triangles on sites  $kl$ , for  $k$  integer, where

$$l = 2l' + v_{LR}t. \quad (35)$$

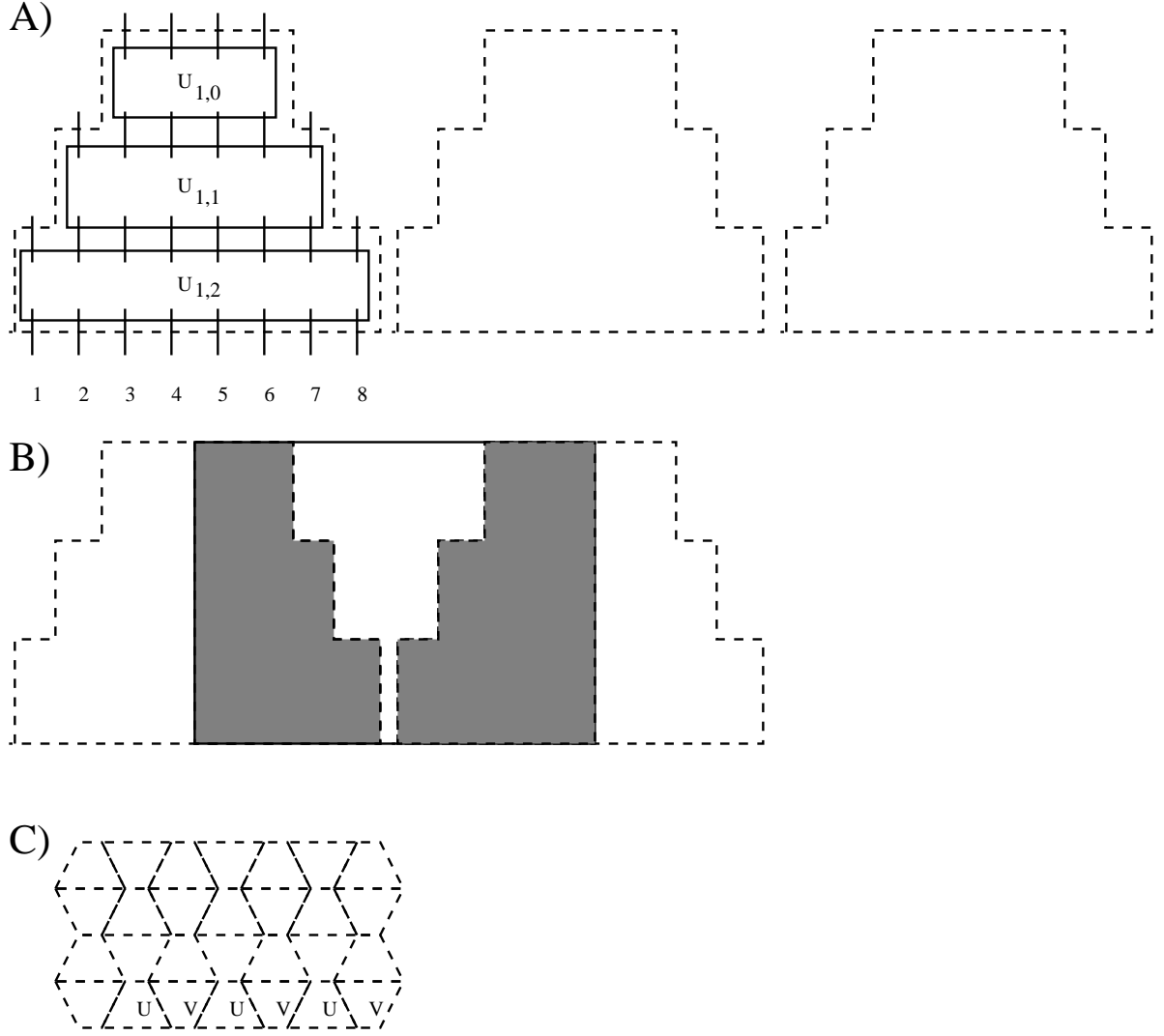


FIG. 9: (a) The dashed lines show the region of space-time used in defining operators  $U_k$ , with space on the horizontal axis and time on the vertical axis. Only three such regions are shown, but the pattern repeats over the entire system. We also show this as a quantum circuit writing  $U_1 = U_{1,0}, U_{1,1}, U_{1,2}$  where each operator  $U_{1,n}$  computes the exponential of the Hamiltonian in a given time slice. Construction is shown for  $l' = 2, n = 3$ . (b) Action of operators  $V_k$  as discussed in text. (c) Iterating many rounds of the corner transfer quantum circuit. On the bottom row we label  $U$  and  $V$ ; on the row above, a  $\tilde{U}$  sits above each  $V$  and a  $\tilde{V}$  above each  $U$ .

Then we define  $U_{k,n}$  for  $0 \leq n \leq n_0 - 1$  by

$$U_{k,n} = \exp[-i \sum_{i=kl-l'/2-n}^{i \leq kl+l'/2+n} h_i(t/2n_0)], \quad (36)$$

and define

$$U_k = U_{k,0} U_{k,1} U_{k,2} \dots U_{k,n_0-1}. \quad (37)$$

We then define the operators  $V_k$  as follows. We define

$$U_{k,n}^L = \exp[-i \sum_{i=kl-l'/2-n}^{kl} h_i(t/2n_0)], \quad (38)$$

$$U_{k,n}^R = \exp[-i \sum_{i=kl}^{kl+l'/2+n} h_i(t/2n_0)].$$

That is,  $U_{k,n}^{L,R}$  represent evolution under the left or right half of the triangles in in Fig. 9(a). Then, we define

$$V_k = \exp(-i \sum_{i=(k+1/2)l-l/2+1}^{(k+1)l+l/2-1} h_i t/2) \left( U_{k,0}^R U_{k,1}^R \dots U_{k,n_0-1}^R \right)^\dagger \left( U_{k+1,0}^L U_{k+1,1}^L \dots U_{k+1,n_0-1}^L \right)^\dagger. \quad (39)$$

That is, each  $V_k$  “undoes” the evolution in the shaded triangles as shown in Fig. 9(b), and then performs the full evolution in the rectangle bordered by the solid line.

We now approximate

$$\exp(-iHt/2) \approx \prod_k V_k \prod_k U_k. \quad (40)$$

Using Lieb-Robinson bounds, one can show that the error in this approximation is

$$\| \exp(-iHt/2) - \prod_k V_k \prod_k U_k \| \leq \mathcal{O}(t \sum_i \|h_i\| \exp(-\mathcal{O}(l'))). \quad (41)$$

In the second step of construction the corner transfer quantum circuit, we define another approximation to  $\exp(-iHt/2)$ . We set

$$\tilde{U}_{k,n} = \exp[-i \sum_{i=(k+1/2)l-l'/2-n}^{i \leq (k+1/2)l+l'/2+n} h_i(t/2n_0)], \quad (42)$$

and define

$$\tilde{U}_k = \tilde{U}_{k,0} \tilde{U}_{k,1} \tilde{U}_{k,2} \dots \tilde{U}_{k,n_0-1}. \quad (43)$$

Here, the centers of the upward facing triangles in Fig. 9(a) are shifted by  $l/2$ , compared to (37). We then define  $\tilde{V}_k$  in analogy to Eq. (39) with the centers again shifted by  $l/2$  and approximate

$$\exp(-iHt/2) \approx \prod_k \tilde{V}_k \prod_k \tilde{U}_k. \quad (44)$$

In Fig. 9(c) we show multiple rounds of the quantum circuit. Except for the row of triangles on the top and bottom boundaries, the quantum circuit looks like diamond-shaped patches in space time. They are rotated 45-degrees from the patches in [7], justifying the name “corner transfer”; the 45-degree rotation is the key improvement over [7] leading to the bound on information propagation (34).

### III. QUANTUM BELIEF PROPAGATION

In this section we apply quantum belief propagation to disordered systems. We begin with a brief review of quantum belief propagation, focusing on the computational effort required, and then discuss modifications for disordered systems. We applied this procedure to two different disordered systems: one a chain with no frustration where Monte Carlo is available for comparison[29], and the other a frustrated spin system with disorder[30].

Quantum belief propagation[22] is a method for constructing a matrix product density operator for a thermal state of a quantum system on a line or other loopless lattice. The algorithm depends on a parameter  $l_0$  and the approximation to the thermal state has the form in one dimension of:

$$\rho = \left( O_{N-l_0+1}^\dagger \dots O_2^\dagger O_1^\dagger \right) \rho_0 \left( O_1 O_2 \dots O_{N-l_0+1} \right), \quad (45)$$

where the operators  $O_i$  act on sites  $i, \dots, i + l_0 - 1$  and the density matrix  $\rho_0$  has the form  $\rho_0 = \rho_0^{1\dots l_0} \otimes \mathbb{1} \otimes \dots \otimes \mathbb{1}$ , with  $\rho_0^{1\dots l_0}$  being a density matrix on sites  $1\dots l_0$ . The implementation of the algorithm depends on tracing out sites, a process analogous to the observations discussed above. Suppose we wish to compute the partition function. If all of the  $O_i$  are the same, as they would be in a system without disorder, then we can consider the completely positive map

$$\rho \rightarrow \text{tr}_1(O_i^\dagger \rho O_i) \otimes \mathbb{1}, \quad (46)$$

where  $\text{tr}_1(\dots)$  denotes a trace over the first site, and  $\rho$  is a density operator on an interval of length  $l_0$ . We start with this map at  $\rho = \rho_0$ , and iterate it until we reach the end of the chain. We then compute the trace of the final  $\rho$  and this is the of the partition function. A similar procedure can be applied to compute expectation values.

The cost of the procedure scales exponentially in  $l_0$ , as it requires diagonalizing matrices of dimension  $2^{l_0}$ [26]. The procedure is effective down to inverse temperatures

$$\beta \sim l_0/v_{LR}. \quad (47)$$

The physical intuition is that the algorithm keeps quantum effects only up to a length scaling  $l_0$ . However, as we will see, the algorithm is capable of keeping track of classical correlations on much longer length scales; this should be no surprise since for classical Hamiltonians which are the sum of commuting operators, such as the Ising Hamiltonian  $H = \sum_i S_i^z S_{i+1}^z$ , quantum belief propagation exactly reproduces classical transfer matrix methods which can exhibit correlation lengths exponentially large in  $\beta$ .

For a disordered system, the operators  $O_i$  may vary as a function of  $i$ , but they depend only on the bonds on sites  $i\dots i + l_0 - 1$ . Below, we consider a system in which the bonds can assume only discrete values; in the first system there are  $2 \cdot 2^{(l_0-1)/2}$  different possible choices for the set of bonds on sites  $i\dots i + l_0 - 1$  while in the second there are  $2^{l_0-1}$  possible choices. We then use the following algorithm: first, we pre-compute the operator  $O$  for each possible choice of bonds. We then randomly generate a configuration of bonds, and iterate the map (46) above, choosing the appropriate  $O$  at each step. This requires an effort which scales linearly in system size.

Interestingly, the algorithm seems to work better at low temperatures on disordered systems than on ordered systems. The reason is probably the following: when deriving the algorithm in [22], we used Lieb-Robinson bounds with velocity  $v_{LR}$ . However, just as in the non-equilibrium case above where the actual velocity  $v_{sw}$  is less than  $v_{LR}$ , in these thermal systems the actual velocity may again be less than  $v_{LR}$ . For systems with disorder, localization effects may further reduce the velocity, and even change the ballistic spreading of the wavepacket to a slower growth. Interestingly, this phenomenon is known by different names in condensed matter, where it is called many-body localization[27], and quantum information theory, where it is called a Lieb-Robinson bound for a disordered system[28].

## A. Results on Disordered Systems

The first disordered system we considered has the Hamiltonian

$$H = \sum_{i=1}^{N/2} J \vec{S}_{2i-1} \cdot \vec{S}_{2i} + \sum_{i=1}^{N/2} J_i S_{2i} \cdot S_{2i+1}, \quad (48)$$

where each spin is spin-1/2,  $J > 0$  and  $J_i = J_F < 0$  with probability  $p$  and  $J_i = J_A > 0$  with probability  $1 - p$ . This model has both ferromagnetic and anti-ferromagnetic couplings, and was proposed to model the compound  $(CH_3)_2CHNH_3Cu(Cl_xBr_{1-x})_3$ , where the probability  $p = x^2$ [33, 34, 35, 36, 37]. The case considered is  $J = 1$  and  $|J_i| = 2$ . We performed simulations on this chain with  $l_0 = 5, 7, 9$  for  $p = 0.2, 0.4, 0.6, 0.8$  and for  $l_0 = 5, 7, 9, 11$  for  $p = 0, 1$ . For the random cases ( $p = 0.2, 0.4, 0.6, 0.8$ ) we considered chains of 100000 sites and computed the uniform susceptibility by the change in partition function in response to a weak applied field. In this way, the susceptibility was self-averaging. For the pure cases, we considered shorter chains, and computed the applied susceptibility by measuring partition functions as in [22]. The results are shown in Figs. 10,11. For small  $l_0$ , qualitatively wrong results are seen at low temperature, with the susceptibility diverging at low enough temperature. However, as  $l_0$  is increased, the accuracy extends to lower temperature. The difference between the curves for  $l_0 = 7$  and  $l_0 = 9$  is small for  $T$  greater than roughly  $1/7$ . In this region also, we agree well with Monte Carlo data.

Data was taken over several different  $\beta$ , with a step of 0.25 in  $\beta$ . As in [22], we set the perturbation  $A$  (following notation of [22]) to equal  $(1/2)(h_{l_0-2, l_0-1} + h_{l_0-1, l_0})$  rather than  $A = h_{l_0-1, l_0}$ .

The second model we considered is [30] a model with frustration and disorder, where quantum Monte Carlo results are not available. The study in [30] was motivated by experimental studies on  $CuGeO_3$ [31] and  $Cu_6Ge_6O_{18-x}H_2O$ [32],

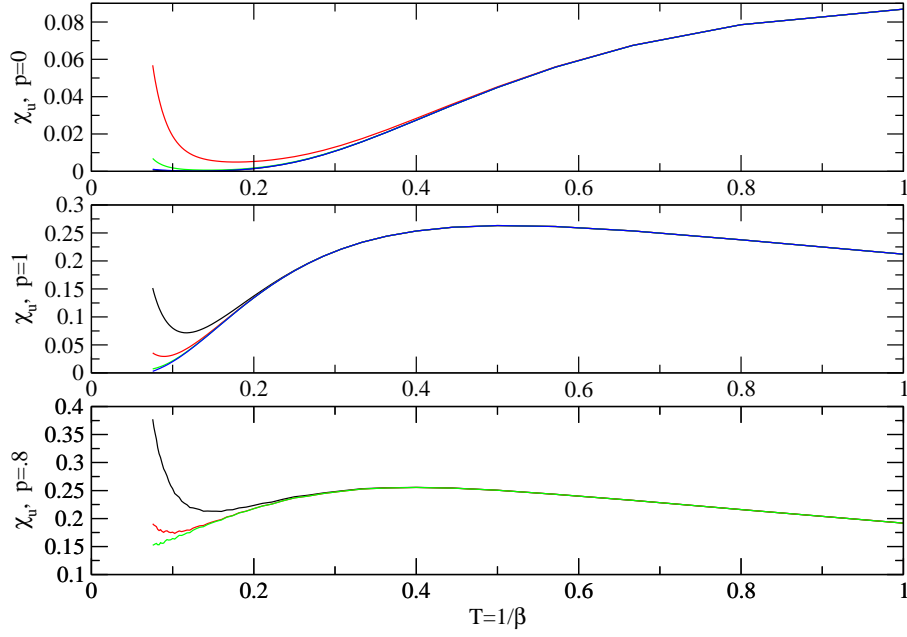


FIG. 10: Uniform susceptibility as a function of temperature for different  $p, l_0$ . Top:  $l_0 = 5$  (black),  $l_0 = 7$  (red),  $l_0 = 9$  (green). Middle:  $l_0 = 5$  (black),  $l_0 = 7$  (red),  $l_0 = 9$  (green),  $l_0 = 11$  (blue). Bottom:  $l_0 = 5$  (black),  $l_0 = 7$  (red),  $l_0 = 9$  (green),  $l_0 = 11$  (blue).

where second neighbor interactions may be important. We were interested in a case where second neighbor interactions would be very important, so we considered the Hamiltonian

$$H = \sum_{i=1}^{N-1} J_i \vec{S}_i \cdot \vec{S}_{i+1} + \sum_{i=1}^{N-2} K_i \vec{S}_i \cdot \vec{S}_{i+2}, \quad (49)$$

and in the pure case we considered  $J_i = 1, K_i = 1/2$ . This is a Majumdar-Ghosh chain with a dimerized ground state. In the disordered case we chose  $J_i = 0.9$  or  $J_i = 1.1$ , with probability  $1/2$  of either choice (similar results were found for choosing  $J = 0.75$  or  $J = 1.25$ ). We choose

$$K_i = (1/2)J_i J_{i+1}, \quad (50)$$

which correlates the second neighbor interaction with the nearest neighbor interaction as described in [29].

We studied  $l_0 = 5, 7, 9$  with chains of length 19999. It is necessary to take such long chains in the pure case to avoid boundary condition effects because at low temperatures in the pure system there is an exponentially increasing correlation length for dimer-dimer correlations. In Fig. 12) we first show the results of the specific heat as a function of  $\beta$  for the pure case, computed from the second derivative of the partition function (probably a very slightly more accurate method is to take the first derivative of the energy as in [22]). A strong difference is seen between  $l_0 = 5$  and  $l_0 = 7$  above  $\beta \sim 3.25$ , but the  $l_0 = 7$  and  $l_0 = 9$  curves are almost identical. This indicates that by going to  $l_0 = 9$  we have succeeded in converging the specific heat in  $l_0$  for  $\beta \leq 10$ .

The uniform susceptibility shows a similar effect. The pure curves show a large difference between  $l_0 = 5$  and  $l_0 = 7, 9$ , but only slight difference can be seen between  $l_0 = 7, 9$  and only above  $\beta = 8$ . Again, the results seem to be converged in  $l_0$  by going to  $l_0 = 9$  in the range of temperatures we consider. The disordered curves show again that  $l_0 = 5$  is too small, but for  $l_0 = 7, 9$  little difference is seen (except for some small random fluctuations) up to  $\beta = 10$ . A very slightly higher susceptibility is seen in the random case compared to the pure case. Finally, we consider the dimer susceptibility, defined by

$$\chi_{dimer} = \beta \left\langle \left( \sum_{i=1}^{N/2-1} \vec{S}_{2i} \cdot \vec{S}_{2i+1} - \vec{S}_{2i+1} \cdot \vec{S}_{2i+2} \right)^2 \right\rangle. \quad (51)$$

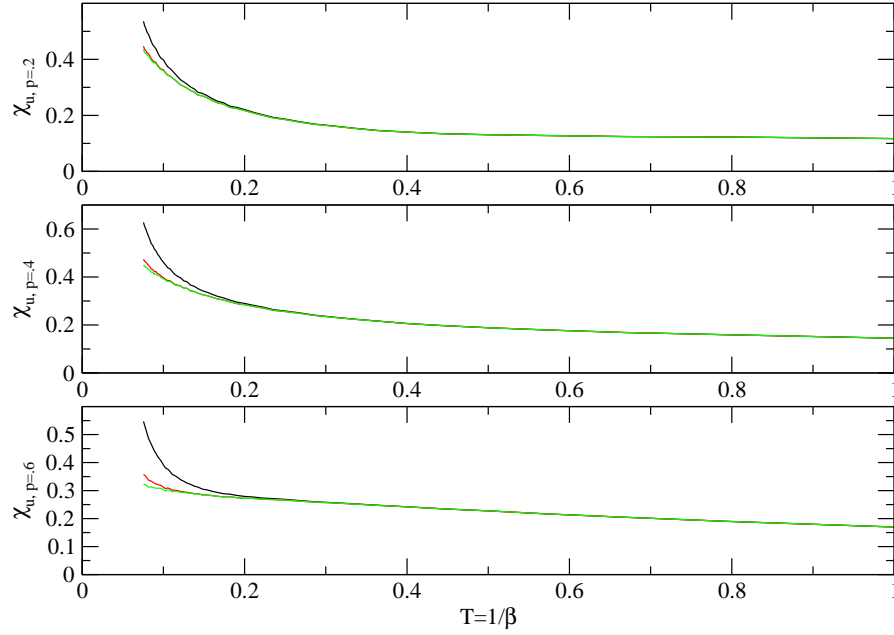


FIG. 11: Uniform susceptibility as a function of temperature for  $p = 0.2, 0.4, 0.6$  from top to bottom and for  $l_0 = 5$  (black),  $l_0 = 7$  (red),  $l_0 = 9$  (green).

This shows a large difference between the pure and disordered cases. The pure cases again show agreement between  $l_0 = 7, 9$  and show an increase that gives  $\chi_{dimer}/\beta$  growing exponentially in  $\beta$ . The disordered cases show  $\chi_{dimer}/\beta$  saturating as a function of  $\beta$ .

The saturation of the dimer-dimer correlation function in the disordered case is no surprise. The disorder locally breaks the  $Z_2$  symmetry between different ordering patterns of the dimers, and is relevant for this one dimensional system. The fact that the uniform susceptibility shows only very slight difference between pure and disordered systems is more surprising; asymptotically, the uniform susceptibility should decay exponentially in  $\beta$  in the pure system and should increase as  $\beta/\log^2(\beta)$  in the random singlet phase[30].

#### IV. DISCUSSION

The main result in this paper is the light-cone quantum circuit method. We have tested this method numerically on a free system, with  $\Delta = 0$ , and on interacting systems with  $\Delta \neq 0$ . We have found decaying oscillations in the expectation value of the spin. In future, this technique will be useful for studying non-integrable systems, to see if they relax to a thermal state[38].

We can study two-dimensional systems by considering them as wide one-dimensional systems; this allows us to double the number of spins, but only leads to a factor of  $\sqrt{2}$  increase in the time compared to direct simulation. Other similar quantum circuit methods may be more effective in two dimensions.

The results using the light-cone quantum circuit method are indeed comparable to those one would find by exactly solving a system of twice the size, at least for  $\Delta = 0$  where we can compute exactly. Thus, we  $l = 18$ , we find results comparable to a system of  $N = 35$  or  $N = 37$  sites. The computational cost to exactly evolve a given system is roughly comparable to that required to do exact diagonalization using Lanczos methods on that system: Lanczos methods and exact evolution both require sparse matrix-vector multiplication, but the number of multiplications needed to reach convergence for the time evolution may be larger than that needed to reach convergence for ground state properties. Thus, we expect that sizes around 35 sites, especially given the low symmetry of the present system, are around the upper limit for exact methods now, while we carried the light-cone quantum circuit method up to  $l = 22$ . Further, the asymptotic analysis of time requirements applies also to memory requirements: the memory requirements of an exact solution on  $N$  sites scale as  $N2^N$ , while the memory requirement of the light-cone quantum circuit method scale as  $l2^l$ , so, regardless of what  $N$  can be obtained using an exact solution, it should be possible to obtain the same  $l$ , up to a difference of a couple sites, in the light-cone quantum circuit method. The main additional cost in the light-cone

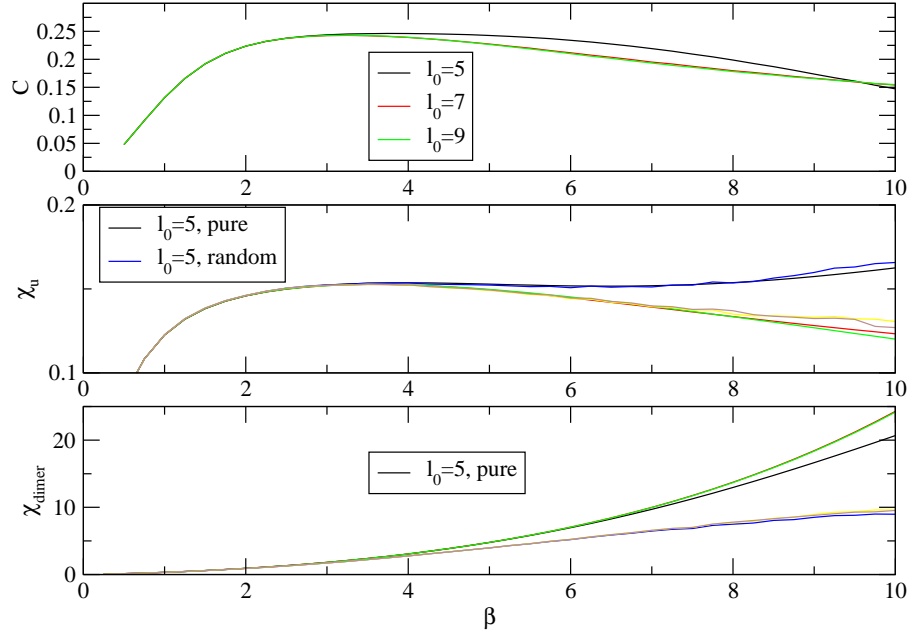


FIG. 12: Top: specific heat for the pure system. Middle: uniform susceptibility for the pure system ( $l_0 = 5, 7, 9$  are black, red, green respectively) and the disordered system ( $l_0 = 5, 7, 9$  are blue, yellow, brown respectively). Bottom: dimer susceptibility for the pure system ( $l_0 = 5, 7, 9$  are black, red, green respectively) and the disordered system ( $l_0 = 5, 7, 9$  are blue, yellow, brown respectively).

quantum circuit method is the need to run many times to obtain statistical samples, but this is a problem which can be parallelized.

*Acknowledgments*— I thank R. Melko for useful comments on implementing sparse matrix-vector multiplication. I thank the KITP for hospitality while this research was conducted. This research was supported in part by the National Science Foundation under Grant No. PHY05-51164. This work supported by U. S. DOE Contract No. DE-AC52-06NA25396.

- 
- [1] U. Schollwoeck, Rev. Mod. Phys. **77**, 259 (2005).
  - [2] F. Verstraete, J. J. Garcia-Ripoll, J. I. Cirac, Phys. Rev. Lett. **93**, 207204 (2004); M. Zwolak and G. Vidal, Phys. Rev. Lett. **93**, 207205 (2004).
  - [3] G. Vidal, Phys. Rev. Lett. **91**, 147902 (2003); G. Vidal, Phys. Rev. Lett. **93**, 040502 (2004).
  - [4] M. B. Hastings, J. Stat. Mech., P08024 (2007).
  - [5] M. B. Hastings, Phys. Rev. B **73**, 085115 (2006).
  - [6] M.M. Wolf, F. Verstraete, M.B. Hastings, and J.I. Cirac, arXiv:0704.3906.
  - [7] T. J. Osborne, Phys. Rev. Lett. **97**, 157202 (2006).
  - [8] E. H. Lieb and D. W. Robinson, Commun. Math. Phys. **28**, 251 (1972).
  - [9] M. B. Hastings and T. Koma, Commun. Math. Phys. **265**, 781 (2006).
  - [10] B. Nachtergaele and R. Sims, Commun. Math. Phys. **265**, 119 (2006).
  - [11] M. B. Hastings, Phys. Rev. B **69**, 104431 (2004).
  - [12] G. Vidal, J. I. Latorre, E. Rico, and A. Kitaev, Phys. Rev. Lett. **90**, 227902 (2003).
  - [13] V. Eisler and I. Peschel, J. Stat. Mech. P06005 (2007).
  - [14] P. Calabrese and J. Cardy, J. Stat. Mech. P10004 (2007).
  - [15] D. Gobert, C. Kollath, U. Schollwoeck, G. Schuetz, Phys. Rev. E **71**, 036102 (2005).
  - [16] S. Bravyi, M. B. Hastings, and F. Verstraete, Phys. Rev. Lett. **97**, 050401 (2006); J. Eisert and T. J. Osborne, Phys. Rev. Lett. **97**, 150404 (2006).
  - [17] G. De Chiara, S. Montangero, P. Calabrese, R. Fazio, J. Stat. Mech. P03001 (2006).
  - [18] P. Calabrese and J. Cardy, J. Stat. Mech. P04010 (2005).
  - [19] S. Ostlund and S. Rommer, Phys. Rev. Lett. **75**, 3537 (1995); M. Fannes, B. Nachtergaele, and R. F. Werner, Comm. Math. Phys. **144**, 443 (1992); F. Verstraete, D. Porras, and J. I. Cirac, Phys. Rev. Lett. **93**, 227205 (2004).

- [20] To understand why  $2^{N/2}$  states suffice, consider how much entanglement is possible across each bond. If we divide the chain of  $N$  sites into a subchain of  $n$  sites and another subchain of  $N - n$  sites, with  $n \leq N - n$ , then there are only  $2^n$  states available on the subchain and so it is possible to perform a Schmidt decomposition and find a matrix product state representation with  $2^n$  states across that bond. The worst case is midway across the chain, when  $n = N/2$ . If we wish to write matrix product operators instead of states, then these estimates are increased to  $4^{N/2}$ .
- [21] M. Cramer, C.M. Dawson, J. Eisert, T.J. Osborne, arXiv:0703314.
- [22] M. B. Hastings, Phys. Rev. B Rapids 76, 201102 (2007).
- [23] X. Wang and T. Xiang, Phys. Rev B **56**, 5061 (1997).
- [24] V. E. Korepin, N. M. Boliubov, and A. G. Izergin, *Quantum Inverse Scattering Method and Correlation Functions*, Cambridge University Press (1993).
- [25] The Krylov space methods may lead to some improvement in the time required compared to the series methods. However, since we are considering a situation in which the entropy increases rapidly, and hence the state  $\exp(iH_L t)\Psi_L$  has very little overlap with  $\Psi_L$ , it seems likely that it would be necessary to take a fairly large  $k$  to obtain accurate results for large  $t$ . Therefore, we are not sure how much advantage would actually be obtained by using Krylov methods here.
- [26] The quantum belief propagation method, as currently implemented, requires manipulating operators, rather than pure states, which increases the computational effort.
- [27] D. M. Basko, I. L. Aleiner, and B. L. Altshuler, Ann. Phys. **321**, 1126 (2006); D. M. Basko, I. L. Aleiner, and B. L. Altshuler, cond-mat/0602510.
- [28] C. K. Burrell, T. J. Osborne, Phys. Rev. Lett. 99, 167201 (2007).
- [29] P. Zhang, Zh. Xu, H. Ying, J. Dai, cond-mat/0502543, conference on "Non-Perturbative Quantum Field Theory: Lattice and Beyond", Guangzhou, P.R. China, Nov. 2004.
- [30] E. Yusuf and Kun Yang, Phys. Rev. B 68, 024425 (2003).
- [31] J. E. Lorenzo et. al. Phys. Rev. B **50**, 1278 (1994).
- [32] M. Hase, K. Ozawa, and N. Shinya, Phys. Rev. B **68**, 214421 (2003).
- [33] H. Manaka, I. Yamada, and H. A. Katori, Phys. Rev. B **63**, 104408 (2001).
- [34] H. Manaka, I. Yamada, and K. Yamaguchi, J. Phys. Soc. Jpn. **66**, 564 (1997).
- [35] H. Manaka and I. Yamada, J. Phys. Soc. Jpn. **66**, 1908 (1997).
- [36] H. Hida, J. Phys. Soc. Jpn. **72**, 688.
- [37] T. Nakamura, J. Phys. Soc. Jpn. **72**, 789 (2003).
- [38] T. Barthel and U. Schollwöck, arXiv:0711.4896.